ICES REPORT 10-24

June 2010

Efficient Algorithms for Multiscale Modeling in Porous Media

by

Mary F. Wheeler, Tim Wildey, and Guangri Xue

The Institute for Computational Engineering and Sciences
The University of Texas at Austin
Austin, Texas 78712

Reference: Mary F. Wheeler, Tim Wildey, and Guangri Xue, "Efficient Algorithms for Multiscale Modeling in Porous Media", ICES REPORT 10-24, The Institute for Computational Engineering and Sciences, The University of Texas at Austin, June 2010.

Efficient Algorithms for Multiscale Modeling in Porous Media*

Mary F. Wheeler† Tim Wildey ‡ Guangri Xue §

Abstract

We describe multiscale mortar mixed finite element discretizations for second order elliptic and nonlinear parabolic equations modeling Darcy flow in porous media. The continuity of flux is imposed via a mortar finite element space on a coarse grid scale, while the equations in the coarse elements (or subdomains) are discretized on a fine grid scale. We discuss the construction of multiscale mortar basis and extend this concept to nonlinear interface operators. We present a multiscale preconditioning strategy to minimize the computational cost associated with contruction of the multiscale mortar basis. We also discuss the use of appropriate quadrature rules and approximation spaces to reduce the saddle point system to a cell-centered pressure scheme. In particular, we focus on multiscale mortar multipoint flux approximation method for general hexahedral grids and full tensor permeabilities. Numerical results are presented to verify the accuracy and efficiency of these approaches.

keywords: multiscale, mortar finite element, domain decomposition, single phase flow, multipoint flux approximation.

1 Introduction

Humans interact with a broad range of natural and engineered subsurface geosystems. They include landfills, contaminated sites, aquifers, nuclear waste repositories, geothermal, and fossil fuel reservoirs. Probably the most widely recognized example is oil and gas production from petroleum reservoirs. Another example is the geologic storage of waste from nuclear reactors. Storage of oil in salt caverns is part of our national security strategy. In addition, the stewardship of water resources requires management of geologic formations, as does the remediation of many types of toxic wastes.

Each geosystem has unique characteristics and challenges. For toxic wastes sites, a central issue is to understand the core processes involved in natural and enhanced bioremediation. For coastal aquifers, the main challenge may be how to optimize long-term

*A portion of this research was supported by the U.S. Department of Energy, Office of Science, Office of Basic Energy Sciences. The Center for Frontiers of Subsurface Energy Security (CFSES) is a DOE Energy Frontier Research Center, under Contract No. DE-SC0001114. The authors gratefully acknowledge the financial support provided by the NSF-CDI under contract number DMS 0835745 and King Abdullah University of Science and Technology (KAUST)-AEA-UTA08-687. Guangri Xue is supported by Award no. KUS-F1-032-04, made by KAUST.

†Center for Subsurface Modeling (CSM), The Institute for Computational Engineering and Sciences (ICES), The University of Texas at Austin, Austin, TX 78712

‡CSM, ICES, The University of Texas at Austin, Austin, TX 78712

§CSM, ICES, The University of Texas at Austin, Austin, TX 78712

productivity through aquifer storage and recovery. In the case of oil and gas production, the goal of the geosystems approach is to optimize the performance of the reservoir, wells, and operations facilities (to create what has been called the "electronic oil field of the future"). Although each geosystem has its unique physics that require site-specific models, all geosystem models will have at their base certain general capabilities to which site-specific capabilities can be added. These general capabilities must include multiscale and multiphysics models and numerical algorithms for approximating the pertinent physical, chemical, geological, and biological processes characteristic of these systems. The underlying processes are complex, involving multiphase flow in porous media, thermal effects, chemical reactions, changing porosities and permeabilities, and bacterial activity. Each process acts primarily on some intrinsic length and time scale but affects dynamics on other scales.

The use of high-performance computing is opening up new opportunities for modeling and understanding complex groundwater systems. Computationally intensive models that describe concentrations and movements of specific contaminants in groundwater are more effective than simple groundwater models in evaluating remediation options. High-performance computing can improve groundwater modeling by providing the ability to (1) use larger and more detailed computational grids, (2) run more simulations under different conditions to evaluate remediation options and determine uncertainty, and (3) develop more complete computational models of physical processes.

Geologic heterogeneity is one of the most important factors affecting subsurface Darcy flow and transport. Although it is difficult to obtain fine-scale heterogeneity information directly by field measurements, geostatistical techniques may be used to generate this information synthetically, with some uncertainty because of the sparsity of field data. Once we generate such data, attempts to resolve fine-scale heterogeneity effects on large three-dimensional field-scale systems can result in large problems, requiring hundreds of millions of grid points. A combination of powerful algorithms and high-performance computers is required for solutions of these systems.

Modeling of these complex subsurface geosystem problems is the major motivation for this work on multiscale mortar mixed finite element methods for treating Darcy flow. Mixed finite element are locally conservative and fluxes are continuous; thus the physics of the flow is modeled correctly. The mortar approach allows the coupling of different physics and/or different algorithms in different subdomains including non-matching grids on subdomain boundaries. In addition, because of the size of many of the reservoirs, efficient solvers are required for the linear and nonlinear systems arising from discretizations. This has led to our focus on the development of domain decomposition algorithms based on multiscale mortar methods

The paper is organized as follows. In Section 2 the mortar mixed finite element method is defined for a linear elliptic model problem. In Section 3, the multiscale interface operator for a substructuring domain decomposition is introduced and an extension to a nonlinear interface operator is formulated. In Section 4, cell-centered methods, including the multipoint flux mixed finite element method (MFMFE), are discussed and the extension to the multiscale mortar MFMFE is formulated. This method has the advantage that it is accurate for both smooth and discontinuous full tensor permabilities. In Section 5, we provide numerical experiments to verify the accuracy of the multiscale mortar MFMFE method on hexahedral grids and demonstrate the effectiveness of a multiscale preconditioner for

slightly compressible single phase flow. In the last section we briefly summarize our results. For convenience, relevant references have been incorporated into the appropriate sections.

2 Model Problem

We consider a computational domain, $\Omega \in \mathbb{R}^d, (d = 2, 3)$, decomposed into a series of nonoverlapping subdomains $\Omega_i, i = 1, 2, \ldots, P$ with interfaces $\Gamma_{ij} = \partial\Omega_i \cap \partial\Omega_j$. We let $\Gamma = \oplus_{1\le i<j\le P}\Gamma_{ij}$ denote the set of interfaces with $\Gamma_i = \partial\Omega_i \cap \Gamma$. The Darcy velocity $\mathbf{u}$ and the pressure p satisfy for $1 \le i \le P$,

$$\begin{cases} \mathbf{u} = -K(\mathbf{x})\nabla p, & \text{in } \Omega_i, \\ \nabla \cdot \mathbf{u} = f, & \text{in } \Omega_i, \\ p = g, & \text{on } \partial\Omega_i \cap \partial\Omega. \end{cases} \tag{1}$$

We assume that there exist positive constants $\hat{c}$, $\hat{C}$, and α_i such that

$$\hat{c}\alpha_i\xi^T\xi \le \xi^T K(\mathbf{x})\xi \le \hat{C}\alpha_i\xi^T\xi, \quad \forall\xi \in \mathbb{R}^d,\ \forall\mathbf{x} \in \Omega_i,\ i = 1, \ldots, P. \tag{2}$$

To couple the subdomain models, we impose the physically meaningful interface conditions on each Γ_{ij},

$$p|_{\Omega_i} = p|_{\Omega_j}, \tag{3}$$

$$\mathbf{u}|_{\Omega_i} \cdot \nu_i + \mathbf{u}|_{\Omega_j} \cdot \nu_j = 0, \tag{4}$$

where ν_i denotes the unit outward normal on $\partial\Omega_i$. These conditions represent continuity of pressure and normal flux and are the basis for the nonoverlapping domain decomposition algorithm to follow.

Let $\mathcal{T}_{h,i}$ be a conforming quasi-uniform affine finite element partition of Ω_i, $1 \le i \le P$, of maximal element diameter h_i. Note that we need quasi-uniformity and conformity only on each subdomain. Our method allows for spatially varying h_i, but to simplify the discussion, we let $h = \max_{1\le i\le P} h_i$ and analyze the method in terms of this single value h. We allow for the possibility that $\mathcal{T}_{h,i}$ and $\mathcal{T}_{h,j}$ do not align on Γ_{ij}. Let

$$\mathbf{V}_{h,i} \times W_{h,i} \subset H(\mathrm{div}, \Omega_i) \times L^2(\Omega_i),$$

be any of the usual mixed finite element spaces (e.g., those of [9, 10, 17, 11, 22]), and let $\mathbf{V}_h$ or, equivalently, $\mathbf{V}_h \cdot \nu$ contain the polynomials of degree k. We assume the approximation order of $W_{h,i}$ is $l + 1$. Then let

$$\mathbf{V}_h = \bigoplus_{i=1}^{P} \mathbf{V}_{h,i}, \quad W_h = \bigoplus_{i=1}^{P} W_{h,i}.$$

Note that the normal components of vectors in $\mathbf{V}_h$ are continuous between elements within each block Ω_i, but not across Γ.

Mortar methods were introduced in [8] as a physically consistent way to weakly couple subdomain models through an interface. The technique is highly flexible and allows for nonmatching grids along each interface as well as different physics in each subdomain. In

this paper we follow the notation from [1] and refer the interested reader to [6, 7, 29] for alternative approaches.

Let the mortar interface mesh $\mathcal{T}_{H,ij}$ be a quasi-uniform finite element partition of Γ_{ij} with maximal element diameter H_{ij}. Let $H = \max_{1\le i,j\le P} H_{ij}$. Denote by $M_{H,ij} \subset L^2(\Gamma_{ij})$ the mortar space on Γ_{ij} containing either the continuous or discontinuous piecewise polynomials of degree q on $\mathcal{T}_{H,ij}$, where q is at least $k+1$. We remark that $\mathcal{T}_{H,ij}$ need not be conforming if $M_{H,ij}$ is discontinuous. Now let,

$$M_H = \bigoplus_{1\le i<j\le P} M_{H,ij}$$

be the mortar finite element space on Γ. For each subdomain Ω_i, define a projection $\mathcal{Q}_{h,i} : L^2(\Gamma_i) \to \mathbf{V}_{h,i}\cdot\nu_i|_{\Gamma_i}$ such that, for any $\phi \in L^2(\Gamma_i)$,

$$\langle \phi - \mathcal{Q}_{h,i}\phi, \mathbf{v}\cdot\nu_i\rangle_{\Gamma_i} = 0, \quad \mathbf{v} \in \mathbf{V}_{h,i}. \tag{5}$$

Throughout this paper, $\|\cdot\|_{r,S}$ is the usual Sobolev norm of $H^r(S)$ (we may drop r if $r = 0$ and S if $S = \Omega$). Following [1], we require that the following condition be satisfied.

Assumption 2.1 *Assume that there exists a constant C, independent of h and H, such that*

$$\|\mu\|_{\Gamma_{ij}} \le C\left(\|\mathcal{Q}_{h,i}\mu\|_{\Gamma_{ij}} + \|\mathcal{Q}_{h,j}\mu\|_{\Gamma_{ij}}\right), \quad \mu \in M_H, \quad 1 \le i < j \le P. \tag{6}$$

Condition (6) says that the mortar space cannot be too rich compared to the normal traces of the subdomain velocity spaces. Therefore, in what follows, we assume that $h \le H \le 1$. Condition (6) is not very restrictive, and is easily satisfied in practice (see, e.g., [20, 30]).

In the mixed finite element approximation of (1), we seek, $\mathbf{u}_h \in \mathbf{V}_h$, $p_h \in W_h$ and $\lambda_H \in M_H$ such that, for each i,

$$\begin{cases} (K^{-1}\mathbf{u}_h, \mathbf{v})_{\Omega_i} = (p_h, \nabla\cdot\mathbf{v})_{\Omega_i} - \langle \lambda_H, \mathbf{v}\cdot\nu_i\rangle_{\Gamma_i} - \langle g, \mathbf{v}\cdot\nu_i\rangle_{\partial\Omega_i\setminus\Gamma}, \\ (\nabla\cdot\mathbf{u}_h, w)_{\Omega_i} = (f, w)_{\Omega_i}, \\ \sum_{i=1}^{P} \langle \mathbf{u}_h\cdot\nu_i, \mu\rangle_{\Gamma_i} = 0, \end{cases} \tag{7}$$

for all $\mathbf{v} \in \mathbf{V}_{h,i}$, $w \in W_{h,i}$ and $\mu \in M_H$.

Strictly within each block Ω_i, we have a standard mixed finite element method with local conservation over each grid cell. Moreover, $\mathbf{u}_h\cdot\nu$ is continuous on any element edge (or face) with weak continuity of the flux across the interfaces with respect to the mortar space M_H.

The following *a priori* error estimate for the mixed finite element (MFEM) solution to (7) first appeared in [3].

Theorem 2.2 *If (6) holds, then there exists a positive constant C, independent of h and H, such that*

$$\|\nabla\cdot(\mathbf{u} - \mathbf{u}_h)\| \le C\sum_{i=1}^{P} \|\nabla\cdot\mathbf{u}\|_{r,\Omega_i} h^r, \tag{8}$$

where $0 \le r \le l+1$, *and*

$$\|\mathbf{u}-\mathbf{u}_h\| \le C\sum_{i=1}^{P}\left(\|p\|_{s+1/2,\Omega_i}H^{s-1/2}+\|\mathbf{u}\|_{r,\Omega_i}h^r+\|\mathbf{u}\|_{r+1/2,\Omega_i}h^rH^{1/2}\right), \tag{9}$$

where $1 \le r \le k+1$, $0 < s \le m+1$. *Furthermore, if full* H^2-*regularity of (1) also holds, then*

$$\|p-p_h\| \le C\sum_{i=1}^{P}\big(\|p\|_{t,\Omega_i}h^t+\|p\|_{s+1/2,\Omega_i}H^{s+1/2}+\|\nabla\cdot\mathbf{u}\|_{t,\Omega_i}h^tH + \|\mathbf{u}\|_{r,\Omega_i}h^rH+\|\mathbf{u}\|_{r+1/2.\Omega_i}h^rH^{3/2}\big), \tag{10}$$

where $1 \le r \le k+1$, $0 < s \le m+1$, *and* $0 \le t \le l+1$.

Remark 2.3 *The* a priori *error estimate motivates a multiscale approach. We choose high order mortar polynomials and balance the subdomain and mortar discretization errors by taking a coarse mortar mesh,* $H = \mathcal{O}(h^\beta), \beta \le 1$. *For example, with* RTN_0 $(k = l = 0)$ *and quadratic mortars* $(m = 2)$, *the errors are balanced if* $H = \mathcal{O}(h^{2/5})$. *Furthermore,* a posteriori *error estimates [19] indicate that this scaling may be overly pessimistic and an optimal balance of errors may be achieved with even coarser or adaptive mortar meshes.*

3 A Multiscale Interface Operator

Using a substructuring domain decomposition algorithm introduced in [14], the linear system resulting from the mortar mixed finite element method (7) can be reduced to a coarse scale interface problem in the mortar space M_H [30, 1, 3].

We define a linear functional $g_H : L^2(\Gamma) \to \mathbb{R}$ by

$$g_H(\mu) = \sum_{i=1}^{P} g_{h,i}(\mu) = \sum_{i=1}^{P}\langle \bar{\mathbf{u}}_h\cdot\nu_i, \mu\rangle_{\Gamma_i},$$

where the pair $(\bar{\mathbf{u}}_h, \bar{p}_h) \in \mathbf{V}_h \times W_h$ solves, for $1 \le i \le P$,

$$\begin{cases} (K^{-1}\bar{\mathbf{u}}_h, \mathbf{v})_{\Omega_i} = (\bar{p}_h, \nabla\cdot\mathbf{v})_{\Omega_i} - \langle g, \mathbf{v}\cdot\nu_i\rangle_{\partial\Omega_i\setminus\Gamma}, & \mathbf{v}\in\mathbf{V}_{h,i},\\ (\nabla\cdot\bar{\mathbf{u}}_h, w)_{\Omega_i} = (f,w)_{\Omega_i}, & w\in W_{h,i}. \end{cases} \tag{11}$$

Similarly, we define a bilinear form $d_H : L^2(\Gamma)\times L^2(\Gamma) \to \mathbb{R}$ by

$$d_H(\lambda,\mu) = \sum_{i=1}^{P} d_{H,i}(\lambda,\mu) = -\sum_{i=1}^{P}\langle \mathbf{u}_h^*(\lambda)\cdot\nu_i, \mu\rangle_{\Gamma_i},$$

where the pair $(\mathbf{u}_h^*(\lambda), p_h^*(\lambda)) \in \mathbf{V}_h \times W_h$ is computed by solving

$$\begin{cases} (K^{-1}\mathbf{u}_h^*(\lambda), \mathbf{v})_{\Omega_i} = (p_h^*(\lambda), \nabla\cdot\mathbf{v})_{\Omega_i} - \langle \lambda, \mathbf{v}\cdot\nu_i\rangle_{\Gamma_i}, & \mathbf{v}\in\mathbf{V}_{h,i},\\ (\nabla\cdot\mathbf{u}_h^*(\lambda), w)_{\Omega_i} = 0, & w\in W_{h,i}, \end{cases} \tag{12}$$

for each $1 \leq i \leq P$ for a given $\lambda \in L^2(\Gamma)$. This gives the coarse scale interface problem,

$$d_H(\lambda_H, \mu) = g_H(\mu), \quad \mu \in M_H. \tag{13}$$

We remark that solving (11) corresponds to solving subdomain problems with zero Dirichlet conditions along the mortar boundaries, and g_H represents the corresponding jump in the flux projected into the mortar space. Solving the coarse scale interface problem (13) amounts to finding the proper mortar values to balance the jump in the flux.

It is straightforward to show (see [14, 1]) that the solution to (7) can be reconstructed from the solution λ_H to the interface problem (13) via

$$\mathbf{u}_h = \mathbf{u}_h^*(\lambda_H) + \bar{\mathbf{u}}_h, \quad p_h = p_h^*(\lambda_H) + \bar{p}_h. \tag{14}$$

The following result concerning the existence and uniqueness of the coarse scale solution has been shown in [1].

Lemma 3.1 *The interface bilinear form $d_H(\cdot,\cdot)$ is symmetric and positive definite on $L^2(\Omega)$. If (6) holds, then $d_H(\cdot,\cdot)$ is positive definite on M_H. Moreover,*

$$d_{H,i}(\mu, \mu) = (K^{-1}\mathbf{u}_h^*(\mu), \mathbf{u}_h^*(\mu))_{\Omega_i} \geq 0. \tag{15}$$

We will find it useful to consider the linear algebraic version of the discrete interface operator. We define a real $N_H \times N_H$ matrix $\mathcal{D}_H$ satisfying

$$[\mathcal{D}_H\lambda, \mu] := d_H(\lambda, \mu) \quad \forall \lambda, \mu \in M_H, \tag{16}$$

where N_H denote the number of degrees of freedom associated with M_H, and $[\cdot,\cdot]$ is the Euclidean scalar product in $\mathbb{R}^{N_H}$. For each $\mu \in M_H$, μ denotes the vector of its values at the N_H nodes. We note that $\mathcal{D}_H = \sum_{i=1}^{P} \mathcal{D}_{H,i}$, where $\mathcal{D}_{H,i}$ satisfy

$$[\mathcal{D}_{H,i}\lambda, \mu] = d_{H,i}(\lambda, \mu) \quad \forall \lambda, \mu \in M_H.$$

The interface problem (13) can be written as

$$\mathcal{D}_H\lambda_H = \mathbf{g}_H, \tag{17}$$

where the operator $\mathcal{D}_H$ is the discrete mortar version of the Steklov-Poincaré operator [21].

3.1 Construction of a multiscale mortar basis

In the original implementation of the mortar mixed finite element method [30, 1, 3], each iteration of conjugate gradient (CG) or general minimum residual (GMRES) method requires the action of the interface operator computed by solving subdomain problems (12) and projecting the flux into the mortar space. In [3], the mortar mixed finite element method is shown to be equivalent to a nonstandard multiscale method. This relationship is exploited in [13], where a multiscale mortar flux basis is computed by solving (12) for each mortar basis function. The multiscale basis functions are constructed by projecting the corresponding boundary fluxes into the mortar space. Then, for each iteration of CG

or GMRES, the action of the interface operator is obtained by taking a linear combinations of the multiscale basis functions.

More precisely, let $\left\{\phi_{H,ij}^{\{k\}}\right\}_{k=1}^{N_{H,ij}}$ denote a basis for the mortar space $M_{H,ij}$ where $N_{H,ij}$ is the number of degrees of freedom associated with $M_{H,ij}$. A multiscale mortar flux basis, is computed by solving (12) with $\lambda = \phi_{H,ij}^{\{k\}}$ on subdomains i and j and projecting the flux response into the mortar space.

We note that in the construction of the multiscale basis, the number of solves on a particular subdomain depends only on the number of mortar degrees of freedom associated with this subdomain. Moreover, the associated flux response for each mortar degree of freedom will be nonzero only on the mortars connected to this subdomain (see [13] for further details).

Once the multiscale basis is computed, the action of the interface operator on every interface iteration is reduced to a linear combination of the basis functions. In [13], this approach is shown to be more efficient than the original matrix-free implementation (even when using a balancing preconditioner [20]), in the case of a large number of subdomains with relatively few mortar degrees of freedom on each interface, or if the permeability is highly heterogeneous.

3.2 Extension to Nonlinear Interface Operators

Many nonlinear subsurface flow problems can be written in terms of a nonlinear interface operator $b : M_H \times M_H \to \mathbb{R}$ where

$$b(\phi, \mu) = \sum_{i=1}^{P} \langle \mathbf{u}(\phi) \cdot \nu_i, \mu \rangle_{\Gamma_i}.$$

For a given ϕ, $\mathbf{u}(\phi)\cdot\nu_i$ is the normal flux obtained by solving a nonlinear subdomain problem with boundary data $p(\phi)$. For example, in the case of slightly compressible single phase flow, the fluid density depends upon the pressure. This gives a nonlinear problem to be solved on each subdomain. We describe this example in detail in Section 5.2.

Following [31], we use an inexact Newton method to solve the nonlinear interface equation,

$$B(\phi) = b(\phi, \mu) = 0.$$

The inexact Newton step $s^{\{k\}} = \phi^{\{k+1\}} - \phi^{\{k\}}$ is computed by solving

$$D_\delta B(\phi^{\{k\}}; \mu) s^{\{k\}} = -B(\phi^{\{k\}}), \tag{18}$$

where the forward difference operator,

$$D_\delta B(\phi; \mu) = \begin{cases} 0, & \mu = 0, \\ \|\mu\| \frac{B(\phi + \delta \|\phi\| \mu/\|\mu\|) - B(\phi)}{\delta \|\phi\|}, & \mu \neq 0, \phi \neq 0, \\ \|\mu\| \frac{B(\delta \mu/\|\mu\|) - B(\phi)}{\delta}, & \mu \neq 0, \phi = 0, \end{cases} \tag{19}$$

is an approximation of $B'(\phi)$. The inexact Newton step is usually approximated using a Newton GMRES algorithm where only the action of the Jacobian is required within each iteration.

Alternatively, we can consider an approach analogous to the construction of the multiscale basis described in Section 3.1. For each Newton iteration we compute,

$$D_\delta B(\phi_{H,ij}^{\{k\}};\mu),$$

for each mortar degree of freedom. As noted in Section 3.1, this approach will require fewer nonlinear subdomain solves than the usual Jacobian-free method if there are large number of subdomains with relatively few mortar degrees of freedom on each interface, or if the permeability is highly heterogeneous.

3.3 A Frozen Jacobian Preconditioner

In many subsurface applications, the heterogeneity of the permeability field dominates the characteristic features of the flow. Furthermore, if the subdomain problems are only mildly nonlinear, as in the case of slightly compressible single phase flow, then we expect the Jacobians to evolve slowly in time. Motivated by these observations, we consider a preconditioning strategy based on a frozen Jacobian.

We select a fixed state $\hat{\phi}$, usually based on the initial conditions, and assemble the Jacobian for this state,

$$\hat{D}_\delta(\hat{\phi},\mu). \tag{20}$$

For each subsequent Newton step, we use an iterative algorithm such as GMRES to solve the preconditioned equation,

$$M^{-1}D_\delta B(\phi^{\{k\}};\mu)s^{\{k\}} = -M^{-1}B(\phi^{\{k\}}),$$

with $M = \hat{D}_\delta(\hat{\phi},\mu)$. Note that for each iteration we require,

- the action of the current Jacobian - computed by solving one nonlinear problem per subdomain,
- the inverse of the preconditioner - computed using the assembled frozen Jacobian without solving subdomain problems.

Clearly, the performance of the preconditioner depends on how closely the frozen Jacobian represents the Jacobian for the current state. This performance can easily be monitored throughout the simulation and a new preconditioner may be constructed at any time based on the current state.

Remark 3.2 *In some situations [27], we can show that the condition number of the preconditioned system is independent of the number of subdomains as well as the subdomain and mortar discretizations. However, this has not been shown for the general nonlinear case.*

4 Cell-centered Subdomain Discretization Methods

In general, we can choose any mixed finite element spaces on the subdomains as they provide accurate and locally mass conservative velocities and handle discontinuous full tensor coefficients well. Standard formulations of MFE give a saddle point systems and require

solving pressure and velocity simultaneously. Another approach is a hybrid MFE formulation [5, 12] that introduces pressure Lagrange multipliers on the element faces, and reduces to a symmetric positive definite system.

More efficient formulations that reduce (11) and (12) to cell-centered pressure schemes have been developed. These are based on appropriate MFE spaces and specific numerical quadrature rule for the velocity mass term, see [23, 24] for diagonal permeability on rectangular grids based on the lowest order Raviart-Thomas (RT_0) MFE method [22], and the expanded mixed finite element (EMFE) for smooth full tensor permeability on rectangular and cuboid grids [4]. For the case of discontinuous permeability, EMFE loses the accuracy unless pressure Lagrange multipliers are introduced along discontinuous interfaces [2]. The multipoint flux mixed finite element (MFMFE) methods [28, 16, 25] are designed to be cell-centered pressure schemes that are accurate for both smooth and discontinuous full tensor permeability.

Numerical quadrature applied to the mass term of (7) is defined element by element as, $\forall \mathbf{q}, \mathbf{v} \in \mathbf{V}_{h,i}$,

$$(K^{-1}\mathbf{q}, \mathbf{v})_{Q,\Omega_i} := \sum_{E \in \mathcal{T}_{h,i}} (K^{-1}\mathbf{q}, \mathbf{v})_{Q,E}.$$

For any element $E \in \mathcal{T}_{h,i}$, there exists a bijection mapping $F_E : \hat{E} \to E$, where $\hat{E}$ is a reference element. Denote the vertices of E and $\hat{E}$ as $\mathbf{r}_i$ and $\hat{\mathbf{r}}_i$ accordingly. Denote the Jacobian matrix as DF_E and its determinant as $J_E = |\det(DF_E)|$. On each element, the numerical quadrature is written as

$$(K^{-1}\mathbf{q}, \mathbf{v})_{Q,E} = \frac{1}{s} \sum_{i=1}^{s} J_E(\hat{\mathbf{r}}_i) K^{-1}\mathbf{q}(\mathbf{r}_i) \cdot \mathbf{v}(\mathbf{r}_i),$$

where s is number of vertices in each element. This quadrature rule is closely related to inner products used in the mimetic finite difference methods [15]. For non-affine elements, such as quadrilaterals and hexahedra, the finite element spaces on $\mathbf{V}_{h,i}$ and $W_{h,i}$ on subdomain Ω_i are given by

$$\begin{aligned} \mathbf{V}_{h,i} &= \left\{ \mathbf{v} \in H(\mathrm{div}, \Omega_i) : \quad \mathbf{v}|_E \leftrightarrow \hat{\mathbf{v}},\ \hat{\mathbf{v}} \in \hat{\mathbf{V}}(\hat{E}), \quad \forall E \in \mathcal{T}_{h,i} \right\}, \\ W_{h,i} &= \left\{ w \in L^2(\Omega_i) : \quad w|_E \leftrightarrow \hat{w},\ \hat{w} \in \hat{W}(\hat{E}), \quad \forall E \in \mathcal{T}_{h,i} \right\}, \end{aligned} \tag{21}$$

where the spaces $\hat{V}(\hat{E})$ and $\hat{W}(\hat{E})$ are classical mixed finite element spaces; and $V(E)$ on any physical element $E \in \mathcal{T}_{h,i}$ are defined via Piola transformation:

$$\mathbf{v} \leftrightarrow \hat{\mathbf{v}} : \mathbf{v} = \frac{1}{J_E} DF_E \hat{\mathbf{v}} \circ F_E^{-1},$$

and $W(E)$ via the standard scalar transformation:

$$w \leftrightarrow \hat{w} : w = \hat{w} \circ F_E^{-1}.$$

The cell-centered multiscale mortar method seeks $\mathbf{u}_h \in \mathbf{V}_h$, $p_h \in W_h$, $\lambda_H \in M_H$ such that for $1 \leq i \leq P$,

$$\begin{aligned}
(K^{-1}\mathbf{u}_h, \mathbf{v})_{Q,\Omega_i} - (p_h, \nabla \cdot \mathbf{v})_{\Omega_i} &= -\langle g, \Pi_R \mathbf{v} \cdot \nu_i \rangle_{\partial\Omega_i / \ \Gamma} \\
&\quad - \langle \lambda_H, \Pi_R \mathbf{v} \cdot \nu_i \rangle_{\Gamma_i}, \quad \forall \mathbf{v} \in \mathbf{V}_{h,i}, \qquad (22) \\
(\nabla \cdot \mathbf{u}_h, w)_{\Omega_i} &= (f, w)_{\Omega_i}, \quad \forall w \in W_{h,i}, \qquad (23) \\
\sum_{i=1}^{P} \langle \Pi_R \mathbf{u}_h \cdot \mathbf{n}_i, \mu \rangle_{\Gamma_i} &= 0, \quad \forall \mu \in M_H, \qquad (24)
\end{aligned}$$

for all $\mathbf{v} \in \mathbf{V}_{h,i}$, $w \in W_{h,i}$ and $\mu \in M_H$.

The equations (22)-(24) give a unified representation of the methods developed in [23, 24] and [26]. For example on rectangular or cuboid grids with diagonal permeability, we get two-point flux approximation scheme [23, 24] by choosing the space $\mathbf{V}_h$ as the RT_0 elements. When the permeability is full tensor, we get MFMFE method [26] by choosing the lowest order Brezzi-Douglas-Marini (BDM_1) [11] space on rectangular grids and by choosing the enhanced lowest order Brezzi-Douglas-Duran-Fortin (BDDF_1) space [16] on cuboid grids.

In the MFMFE method, Π_R denotes RT_0 projection operator [22, 17] and is necessary to maintain accuracy. The reason, roughly speaking, is that the numerical quadrature has first order accuracy when the space is restricted to the lower order space. In consequence, having Π_R in (24) keeps the symmetry of the method and also guarantees the existence of the solution of (22)-(24). The accuracy of the mortar multiscale MFMFE method (22)-(24) on both affine, quadrilateral, and hexahedral grids is analyzed in [26]. In such case, modification of the interface operator in Section 3 is straightforward by adding the interpolation operator Π_R.

In the next section, we employ cell-centered method as subdomain discretization. In the first example, we consider MFMFE method as subdomain discretization that handle full permeability tensor and hexahedral grids. In the second example, we consider diagonal permeability on cuboid grids, and it is sufficient to employ two-point flux approximation scheme [23, 24].

5 Numerical Results

5.1 Multiscale Mortar MFMFE Method on Hexahedral Grids

In this section we provide a numerical experiment that shows the accuracy of the multiscale mortar MFMFE method. We choose full permeability tensor

$$K = \begin{pmatrix} x^2 + (y+2)^2 & 0 & \cos(xy) \\ 0 & z^2 + 2 & \sin(yz) \\ \cos(xy) & \sin(yz) & (y+3)^2 \end{pmatrix}$$

and solve the problem (1) with given analytical solution

$$p(x, y, z) = x^4 y^3 + x^2 + yz^2 + \cos(xy)\sin(z).$$

We take the domain to be a C^∞ map of unit cube. The map is defined as

$$x = \hat{x} - 0.03\cos(3\pi\hat{x})\cos(3\pi\hat{y})\cos(3\pi\hat{z}),$$
$$y = \hat{y} + 0.04\cos(3\pi\hat{x})\cos(3\pi\hat{y})\cos(3\pi\hat{z}),$$
$$z = \hat{z} + 0.05\cos(3\pi\hat{x})\cos(3\pi\hat{y})\cos(3\pi\hat{z}).$$

The domain is divided into eight equal-sized subdomains with interfaces along $x = 0.5$, $y = 0.5$, and $z = 0.5$. The computational grids on different levels are defined by mapping uniform refinements of a reference grid on unit cube. More precisely, each physical hexahedral element is defined through trilinear mapping of cuboid element. For the initial grid, we use a $2 \times 2 \times 2$ subdomain grid. The initial mortar grids all have one element. For the case of linear mortars, we refine subdomain and mortar elements by half in each direction on each level of grid refinement, which gives $H = 2h$. For the case of quadratic mortars, we divide subdomain element by four in each direction and divide mortar element by half in each direction, which gives $H = h^{1/2}$.

The boundary conditions on $\hat{x} = 0$ and $\hat{x} = 1$ are Dirichlet and the other four boundaries are of Neumann. The boundary values are computed from the analytic solution. We use conjugate gradient method to solve the interface problem. The stopping criteria of conjugate iteration is that relative residual is smaller than 10^{-9}. We report L^2 norm of pressure error $\|p - p_h\|$ and velocity error $\|\mathbf{u} - \mathbf{u}_h\|$. The triple norm $|||p - p_h|||$ is computed by the midpoint quadrature rule. We also report number conjugate iterations arising in the interface problem.

Table 1: Discontinuous linear mortars and matching grids

$1/h$	$\|p - p_h\|$		$\|\mathbf{u} - \mathbf{u}_h\|$		$\|\|\|p - p_h\|\|\|$		CGIter	Mortar DOF
4	2.76E-01	–	3.08E+00	–	4.12E-02	–	25	12
8	1.34E-01	1.04	1.69E+00	0.87	9.73E-03	2.08	33	48
16	6.67E-02	1.01	9.04E-01	0.90	2.85E-03	1.77	47	192
32	3.33E-02	1.00	4.62E-01	0.97	7.74E-04	1.88	68	768
64	1.67E-02	1.00	2.31E-01	1.00	1.98E-04	1.97	98	3072

Table 2: Discontinuous quadratic mortars and matching grids

$1/h$	$\|p - p_h\|$		$\|\mathbf{u} - \mathbf{u}_h\|$		$\|\|\|p - p_h\|\|\|$		CGIter	Mortar DOF
4	2.76E-01	–	3.08E+00	–	4.12E-02	–	25	27
16	6.67E-02	1.02	9.04E-01	0.88	2.85E-03	1.93	45	108
64	1.67E-02	1.00	2.31E-01	0.98	1.98E-04	1.92	91	432

Table 1 and Table 2 show the convergence behavior with discontinuous linear mortars and discontinuous quadratic mortars. Both the velocity and pressure have first order con-

vergence. We observe some superconvergence of pressure in both cases. Quadratic mortars are more efficient than linear mortars in terms of number of degrees of freedom (DOF). Maintaining the same accuracy, quadratic mortars only require 432 DOF per subdomain on the finest level but linear mortars require 3072 DOF. Fig 1 shows the solution and error profile for discontinuous linear mortars.

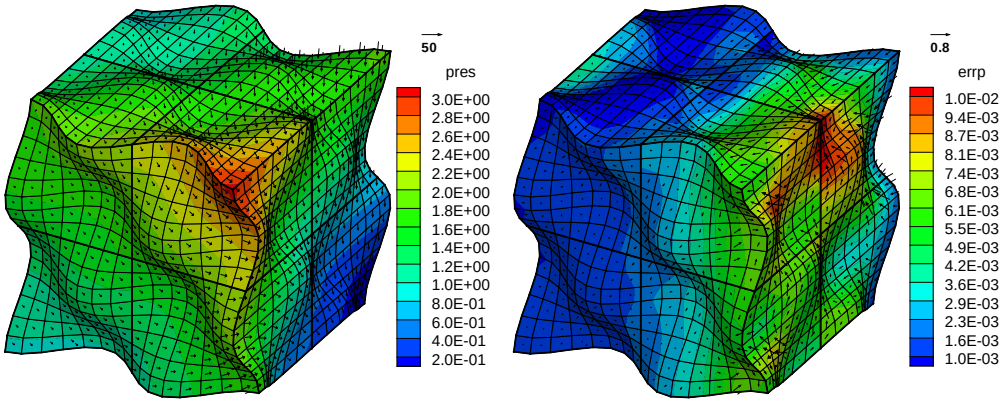

Figure 1: Multiscale Mortar MFMFE solution (left) and error (right): discontinuous linear mortars.

5.2 Slightly Compressible Single Phase Flow

Slightly compressible single phase flow is modeled using the conservation of mass equation,

$$\frac{\partial}{\partial t}(\phi\rho) + \nabla \cdot \mathbf{u} = q, \tag{25}$$

where ϕ is the porosity, ρ is the density, q is the source term, and $\mathbf{u}$ is the Darcy velocity given by,

$$\mathbf{u} = -\frac{K}{\mu}\rho\left(\nabla p - \rho g \nabla \mathcal{D}\right). \tag{26}$$

Here K is the permeability tensor, p is the water pressure, μ is the viscosity, g is the magnitude of the gravitational acceleration, and $\mathcal{D}$ is the depth. The water density, $\rho = \rho(p)$, satisfies the equation of state,

$$\rho = \rho^{\text{ref}} e^{c_f(p - p^{\text{ref}})}, \tag{27}$$

where ρ^{ref} is the reference density, p^{ref} is the reference pressure, and c_f is the compressibility. The nonlinearity of this model is rather modest since the compressibility is usually small.

For boundary conditions, we assume $\mathbf{u}\cdot\nu_i = 0$ on $\partial\Omega_i\backslash\Gamma$. Thus, we define the constrained spaces for the velocities,

$$\mathbf{V}_{h,i,0} = \{\mathbf{v} \in \mathbf{V}_{h,i} \mid \mathbf{v}\cdot\nu_i = 0, \text{ on } \partial\Omega_i\backslash\Gamma\}.$$

and $\mathbf{V}_{h,0} = \bigoplus_{i=1}^{P} \mathbf{V}_{h,i,0}$. Define $0 = t_0 < t_1 < \ldots$, $\Delta t^m = t_m - t_{m-1}$, and $f^m = f(t_m)$ for any sufficiently smooth function f. The backward Euler mortar mixed finite element

method for (25)-(26) seeks $\mathbf{u}_h^m \in \mathbf{V}_{h,0}$, $p_h^m \in W_h$, $\lambda_H^m \in M_H$ such that for $1 \leq i \leq P$,

$$\left(\left(\frac{K\rho_h^m}{\mu}\right)^{-1}\mathbf{u}_h^m, \mathbf{v}\right)_{Q,\Omega_i} - (p_h^m, \nabla\cdot\mathbf{v})_{\Omega_i} + (\rho_h^m g\mathbf{e}_x, \nabla\cdot\mathbf{v})_{\Omega_i} = -\langle\lambda_H^m, \mathbf{v}\cdot\nu_i\rangle_{\Gamma_i}, \quad \forall\mathbf{v}\in\mathbf{V}_{h,i,0}, \tag{28}$$

$$\left(\phi\frac{\rho_h^m - \rho_h^{m-1}}{\Delta t^m}, w\right) + (\nabla\cdot\mathbf{u}_h^m, w)_{\Omega_i} = (q^m, w)_{\Omega_i}, \qquad \forall w\in W_{h,i}, \tag{29}$$

$$\sum_{i=1}^{P}\langle\mathbf{u}_h^m\cdot\mathbf{n}_i, \mu\rangle_{\Gamma_i} = 0, \qquad \forall\mu\in M_H. \tag{30}$$

where $\rho_h^m = \rho(p_h^m)$ and $\mathbf{e}_x$ is the unit vector in the x-direction..

In this example, we use the permeability field from the 10$^{\text{th}}$ SPE Comparative Solution Project. The computational domain is 100[ft] $\times$ 2200[ft] $\times$ 1200[ft]. We upscale the permeability field to 33,000 elements and divide the domain into 55 equal sized subdomains each containing 600 elements as shown in Fig. 2. Each mortar is either 100[ft] $\times$ 200[ft] in the xz-plane or 100[ft] $\times$ 240[ft] in the xy-plane. Each mortar mesh contains 4 elements (2×2) and uses continuous quadratic mortars giving 25 degrees of freedom per mortar.

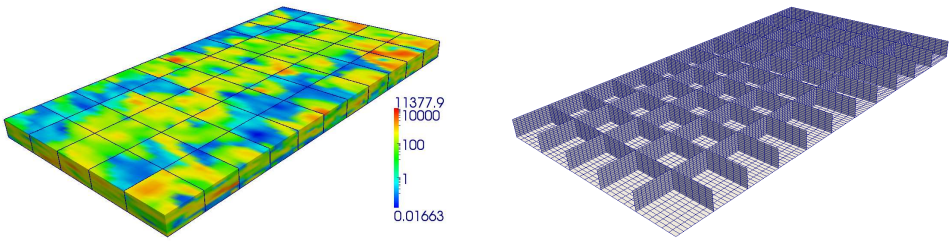

Figure 2: Logarithm of the SPE10 permeability field and subdomain decomposition (left) and cross sections showing each subdomain grid (right) in Example 3.

The initial reservoir pressure at the top is 500[psi] and a hydrostatic pressure is used throughout the reservoir. An injection well, modeled using Peaceman's approximation [18], is located at each corner and the bottom hole pressure is gradually increased from 650[psi] to 1000[psi] over 50 days. At the center of the reservoir is a production well where the bottom hole pressure gradually decreases from 500[psi] to 350[psi] over 50 days. We simulate for 50 days with a uniform time step of 1.0 days. Fig. 3 shows the reservoir pressure and the fluid density after the 50 days.

Our goal is to compare the computational cost and the simulation time for the following three methods:

- **Method 1:** Original nonoverlapping domain decomposition method where the interface Newton update is computed using an inexact matrix-free Newton-GMRES

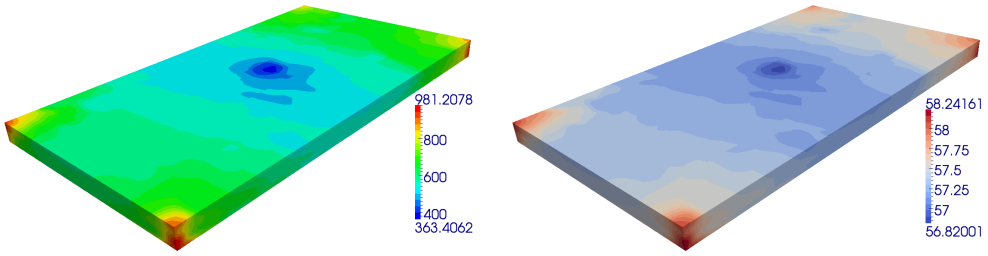

Figure 3: Multiscale mortar MFEM pressure solution (left) and fluid density (right) in Example 3.

algorithm.

- **Method 2:** Multiscale method where the interface Jacobian is assembled for each linearization.
- **Method 3:** Multiscale preconditioner approach where the interface Jacobian is assembled at the initial time and used as a preconditioner for subsequent interface Jacobians.

Table 3 gives the average number of solves per subdomain per interface Newton step, the time required to compute each Newton step, and the total simulation time. Due to the relatively large number of subdomains and the highly heterogenous permeability field, Method 1 requires nearly 200 GMRES iterations to compute each interface Newton update. On the other hand, the number of subdomain solves for Method 2 depends only on the number of degrees of freedom in the mortar space and therefore is independent of the number of subdomains and the permeability field. This results in a much more efficient algorithm. Finally, since the problem is only mildly nonlinear and the flow is dominated by

Table 3: The average number of nonlinear solves per subdomain, the computation time for each interface Newton step, and the total simulation time.

	Avg. Solves	Time/Newton (s)	Sim. Time (s)
Method 1	197.1	294.8	15627.5
Method 2	101	66.6	3396.6
Method 3	5.0	29.1	1545.4

the heterogeneities in the permeability field, the interface Jacobians do not change much throughout time and Method 3, which uses the initial Jacobian as a preconditioner, performs the best. In Table 3, we do not report the number of subdomain solves to assemble the preconditioner since this is performed only once. The time required to assemble the multiscale preconditioner is approximately 64 seconds and has been included in the total solution time. We also remark that the application of the preconditioner is nontrivial and

for this example requires approximately 248 seconds, nearly 25% of the total simulation time. However, the reduction in the number of interface iterations per Newton step more than compensates for this additional cost.

6 Conclusions

This paper has focused on accurate and efficient physics-driven algorithms for modeling Darcy flow in porous media. We have described the multiscale mortar MFMFE method for coupling different hexahedra subdomains with different grids. Computational results have been presented confirming convergence. In addition, we have demonstrated the robustness and effectiveness of a multiscale preconditioners for slightly compressible single phase flow. Current work is in progress to extend this methodology to two and three phase flow problems.

References

[1] T. Arbogast, L. C. Cowsar, M. F. Wheeler, and I. Yotov. Mixed finite element methods on nonmatching grid blocks. *SIAM J. Numer. Anal.*, 37:1295–1315, 2000.

[2] T. Arbogast, C. N. Dawson, P. T. Keenan, M. F. Wheeler, and I. Yotov. Enhanced cell-centered finite differences for elliptic equations on general geometry. *SIAM J. Sci. Comp.*, 19(2):404–425, 1998.

[3] T. Arbogast, G. Pencheva, M. F. Wheeler, and I. Yotov. A multiscale mortar mixed finite element method. *Multiscale Model. Simul.*, 6(1):319–346, 2007.

[4] T. Arbogast, M. F. Wheeler, and I. Yotov. Mixed finite elements for elliptic problems with tensor coefficients as cell-centered finite differences. *SIAM J. Numer. Anal.*, 34(2):828–852, 1997.

[5] D. N. Arnold and F. Brezzi. Mixed and nonconforming finite element methods: Implementation, postrpocessing and error estimates. *Mathematical Modeling and Numerical Analysis*, 19(1):7–32, 1985.

[6] F. B. Belgacem. The mortar finite element method with Lagrange multipliers. *Numer. Math.*, 84(2):173–197, 1999.

[7] F. B. Belgacem. The mixed mortar finite element method for the incompressible stokes problem: Convergence analysis. *SIAM J. Numer. Anal.*, 37(4):1085–1100, 2000.

[8] C. Bernardi, Y. Maday, and A. T. Patera. A new nonconforming approach to domain decomposition: the mortar element method. In *Nonlinear partial differential equations and their applications. Collège de France Seminar, Vol. XI (Paris, 1989–1991)*, volume 299 of *Pitman Res. Notes Math. Ser.*, pages 13–51. Longman Sci. Tech., Harlow, 1994.

[9] F. Brezzi, J. Douglas, R. Durán, and M. Fortin. Mixed finite elements for second order elliptic problems in three variables. *Numer. Math.*, 51(2):237–250, 1987.

[10] F. Brezzi, J. Douglas, M. Fortin, and L. D. Marini. Efficient rectangular mixed finite elements in two and three space variables. *RAIRO Modél. Math. Anal. Numér.*, 21(4):581–604, 1987.

[11] F. Brezzi, J. Douglas, and L. D. Marini. Two families of mixed finite elements for second order elliptic problems. *Numer. Math.*, 47(2):217–235, 1985.

[12] F. Brezzi and M. Fortin. *Mixed and Hybrid Finite Element Methods*. Spring-Verlag, New York, 1991.

[13] B. Ganis and I. Yotov. Implementation of a mortar mixed finite element method using a multiscale flux basis. *Comput. Methods Appl. Mech. Engrg.*, 198:3989–3998, 2009.

[14] R. Glowinski and M. F. Wheeler. Domain decomposition and mixed finite element methods for elliptic problems. In R. Glowinski, G. H. Golub, G. A. Meurant, and J. Periaux, editors, *First International Symposium on Domain Decomposition Methods for Partial Differential Equations*, pages 144–172. SIAM, 1988. Philadelphia.

[15] J. Hyman, M. Shashkov, and S. Steinberg. The numerical solution of diffusion problem in strongly heterogeneous non-isotropic materials. *Journal of Computational Physics*, 132:130–148, 1997.

[16] R. Ingram, M. F. Wheeler, and I. Yotov. A multipoint flux mixed finite element method on hexahedra. Technical Report TR-MATH 09-22, Dept. Math., University of Pittsburgh, Submitted to SIAM J. Numer. Anal., 2009.

[17] J.-C. Nédélec. Mixed finite elements in $\mathbf{R}^3$. *Numer. Math.*, 35(3):315–341, 1980.

[18] D. W. Peaceman. Interpretation of well-block pressures in numerical reservior simulation. *SPE6893, The 52nd Annual Fall Technical Conference and Exhibition, Denver, CO*, 1977.

[19] G. Pencheva, M. Vohralik, M. F. Wheeler, and T. Wildey. Robust a posteriori error control and adaptivity for multiscale, multinumerics, and mortar coupling. Preprint, 2010.

[20] G. Pencheva and I. Yotov. Balancing domain decomposition for mortar mixed finite element methods on non-matching grids. *Numer. Linear Algebra Appl.*, 10:159–180, 2003.

[21] A. Quarteroni and A. Valli. *Domain Decomposition Methods for Partial Differential Equations*. Oxford University Press, UK, 2005.

[22] R. A. Raviart and J. M. Thomas. A mixed finite element method for 2nd order elliptic problems. In *Mathematical Aspects of the Finite Element Method, Lecture Notes in Mathematics*, volume 606, pages 292–315. Springer-Verlag, New York, 1977.

[23] T. Russell and M. Wheeler. Finite element and finite difference method for continuous flows in porous media. *Frontiers in Applied Mathematics*, 1:35, 1983.

[24] A. Weiser and M. F. Wheeler. On convergence of block-centered finite differences for elliptic problems. *SIAM J. on Numer. Anal.*, 25:351–375, 1988.

[25] M. Wheeler, G. Xue, and I. Yotov. Multipoint flux mixed finite element method on distorted quadrilaterals and hexahedra. Preprint, 2010.

[26] M. Wheeler, G. Xue, and I. Yotov. A multiscale mortar multipoint flux mixed finite element method. Preprint, 2010.

[27] M. F. Wheeler, T. Wildey, and I. Yotov. A multiscale preconditioner for stochastic mortar mixed finite elements. Preprint, 2010.

[28] M. F. Wheeler and I. Yotov. A multipoint flux mixed finite element method. *SIAM. J. Numer. Anal.*, 44(5):2082–2106, 2006.

[29] B. I. Wohlmuth. A mortar finite element method using dual spaces for the lagrange multiplier. *SIAM J. Numer. Anal.*, 38(3):989–1012, 2001.

[30] I. Yotov. *Mixed finite element methods for flow in porous media.* PhD thesis, Rice University, Houston, TX, 1996. Also TR96-09, Department of Computational and Applied Mathematics, Rice University and TICAM report 96-23, University of Texas at Austin.

[31] I. Yotov. A multilevel Newton-Krylov interface solver for multiphysics couplings of flow in porous media. *Numerical Linear Algebra with Applications*, 8(8):551–570, 2001.